Particle size segregation in granular avalanches: A brief review of recent progress

J.M.N.T. Gray

School of Mathematics and Manchester Centre for Nonlinear Dynamics, University of Manchester, Manchester, M13 9PL, United Kingdom

Abstract. Hazardous natural flows such as snow avalanches, debris-flows, lahars and pyroclastic flows are part of a much wider class of granular avalanches, that frequently occur in industrial processes and in our kitchens! Granular avalanches are very efficient at sorting particles by size, with the smaller ones percolating down towards the base and squeezing the larger grains up towards the free-surface, to create inversely-graded layers. This paper provides a short introduction and review of recent theoretical advances in describing segregation and remixing with relatively simple hyperbolic and parabolic models. The derivation from two phase mixture theory is briefly summarized and links are drawn to earlier models of Savage & Lun and Dolgunin & Ukolov. The more complex parabolic version of the theory has a diffusive force that competes against segregation and yields S-shaped steady-state concentration profiles through the avalanche depth, that are able to reproduce results obtained from particle dynamics simulations. Time-dependent exact solutions can be constructed by using the Cole-Hopf transformation to linearize the segregation-remixing equation and the nonlinear surface and basal boundary conditions. In the limit of no diffusion, the theory is hyperbolic and the grains tend to separate out into completely segregated inversely graded layers. A series of elementary problems are used to demonstrate how concentration shocks, expansion fans, breaking waves and the large and small particles paths can be computed exactly using the model. The theory is able to capture the key features of the size distribution observed in stratification experiments, and explains how a large particle rich front is connected to an inversely graded avalanche in the interior. The theory is simple enough to couple it to the bulk flow field to investigate *segregation-mobility* feedback effects that spontaneously generate self-channelizing leveed avalanches, which can significantly enhance the total run-out distance of geophysical mass flows.

Keywords: avalanches, debris-flows, segregation, mixing, shocks, diffusion, recirculation
PACS: 61.43.-j; 62.50.Ef; 64.75.Ef; 64.75.St; 92.40.Gc; 92.40.Ha; 92.40.vw

INTRODUCTION

As a body of grains avalanches downslope it dilates, in order for the particles to shear past one another, and the upper layers of the flow move faster than the lower ones, as shown in the schematic diagram in figure 1. The combination of velocity shear and dilation, acts as a random fluctuating sieve [1], which allows the smaller particles to preferentially percolate down into gaps that open up beneath them under the action of gravity, since they are more likely to fit into the available space than the large grains. Once the smaller particles get underneath they exert a force that squeeze the larger grains upwards. The combination of *kinetic sieving* and *squeeze expulsion* [1] causes the particles to segregate into layers, which have greater concentrations of large particles near the free-surface and higher concentrations of fines near the base of the flow. In geology this is known as *inverse grading* [2] and is often associated with granular flows [3]. The inverse grading of the particle size distribution is not necessarily preserved in avalanche deposits, which can be very complex [4]. Indeed, even a relatively simple two-dimensional inversely graded flow with deposition yields a deposit that is *normally graded* [5] with the fines above the large particles.

Large particles that rise to the upper faster moving layers of the avalanche, tend to be transported to the flow front. Here they are often overrun, but rise to the surface again by particle size segregation. This *recirculation* allows bouldery flow fronts to develop in hazardous geophysical mass flows, such as debris-flows, pyroclastic flows and wet and dry snow avalanches [6–9], which give rise to interesting *segregation-mobility* feedback effects [5]. Larger less mobile particles at the flow front are shouldered to the side by the more mobile interior, to create static coarse grained lateral *levees* [10] that channelize the flow and enhance the total run-out distance. Such segregation mobility feedback effects are also responsible for fingering instabilities on chutes [11–13] and digitate lobate terminations [14].

Granular avalanches frequently occur in much smaller scale processes, such as rotating tumblers, where different modes of deposition create a rich variety of patterns, including Catherine wheels [15], leafs [16] and petals [17, 18]. Similar deposition mechanisms are responsible for the formation of stratification and segregation patterns in heaps

CP1227, *IUTAM-ISIMM Symposium on Mathematical Modeling and Physical Instances of Granular Flows,*
edited by J. Goddard, J. T. Jenkins, and P. Giovine

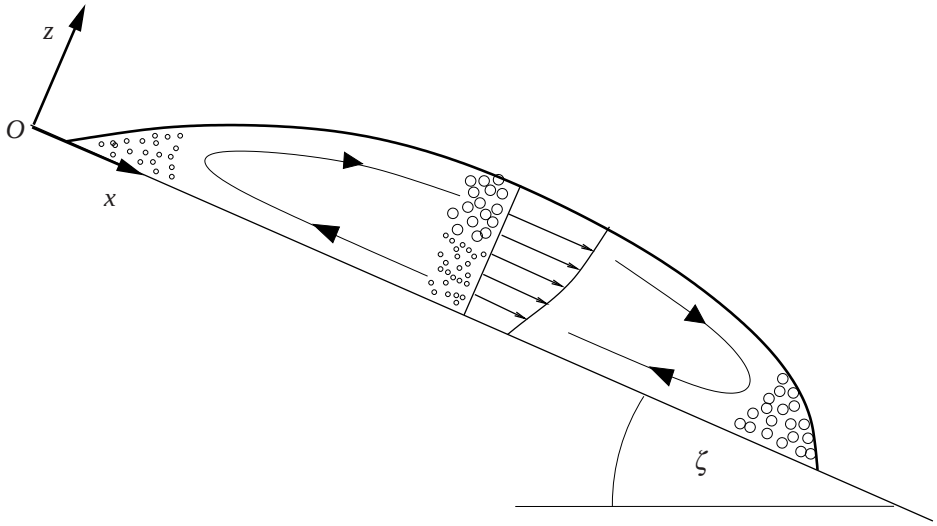

FIGURE 1. A sketch of an avalanche flowing down a plane inclined at an angle ζ to the horizontal. The x axis points down the chute, the z axis is normal to the plane and the y axis goes into the page. The particle size distribution and the downslope velocity profile are illustrated schematically. Large particles tend to rise to the faster moving surface layers, and are transported to the flow front, where they can be recirculated.

and silos [5, 15, 19, 20]. Size segregation is therefore of considerable practical importance to the pharmaceutical, bulk chemical, mining and food industries. Sometimes it is useful, such as in the mineral processing industry, but often it is a source of inconsistency and poor quality and the aim is then to minimize its effect. This paper provides a brief review of recent progress in modelling the particle size segregation process in a bi-disperse avalanche using a relatively simple approach.

DERIVATION OF THE SEGREGATION-REMIXING EQUATION

The segregation-remixing equation can be derived [16, 21, 22] from binary or ternary mixture theory. Here we follow Gray and Chugunov [16]'s derivation, which assumes that the mixture is composed of *large* and *small* particles and that the interstitial pore space is subsumed into the volume fractions, ϕ^l and ϕ^s, of large and small particles per unit mixture volume. This implicity assumes that the solids volume fraction is approximately constant within the avalanche, which is a reasonable first approximation. By definition the volume fractions $\phi^s, \phi^l \in [0,1]$ and they sum to unity

$$\phi^l + \phi^s = 1. \tag{1}$$

Mixture theory defines overlapping partial densities, ρ^μ, partial velocities, $\mathbf{u}^\mu$, and partial pressures, p^μ, for each of the constituents $\mu = l,s$ per unit mixture volume. Each of the constituents satisfies individual mass and momentum conservation laws [e.g. 23, 24]

$$\frac{\partial \rho^\mu}{\partial t} + \nabla \cdot (\rho^\mu \mathbf{u}^\mu) = 0, \qquad \mu = l,s, \tag{2}$$

$$\frac{\partial}{\partial t}(\rho^\mu \mathbf{u}^\mu) + \nabla \cdot (\rho^\mu \mathbf{u}^\mu \otimes \mathbf{u}^\mu) = -\nabla p^\mu + \rho^\mu \mathbf{g} + \mathbf{B}^\mu, \qquad \mu = l,s, \tag{3}$$

where $\otimes$ is the dyadic product, $\rho^\mu \mathbf{g}$ is the gravitational force and $\mathbf{B}^\mu$, is the force exerted on phase μ by the other constituent. The interaction forces in a binary mixture are equal and opposite to one another, $\mathbf{B}^l = -\mathbf{B}^s$, and cancel out in the bulk mass and momentum balances, which are obtained by summing (2) and (3) over all constituents. It is useful to define the bulk density ρ, bulk velocity $\mathbf{u}$ and bulk pressure p as

$$\rho = \rho^l + \rho^s, \quad \rho \mathbf{u} = \rho^l \mathbf{u}^l + \rho^s \mathbf{u}^s, \quad p = p^l + p^s. \tag{4}$$

The partial and intrinsic densities are related by a linear volume fraction scaling [24], while the partial and intrinsic velocity fields are identical

$$\rho^{\mu} = \phi^{\mu}\rho^{\mu *}, \quad \mathbf{u}^{\mu} = \mathbf{u}^{\mu *}, \tag{5}$$

where the superscript $*$ denotes an intrinsic variable. A coordinate system *Oxyz* is defined, with the *x*-axis pointing down a chute inclined at an angle ζ to the horizontal, the *y*-axis across the chute and the *z*-axis as the upward pointing normal as shown in figure 1. The constituent velocity $\mathbf{u}^{\mu}$ and the bulk velocity $\mathbf{u}$ have components $(u^{\mu}, v^{\mu}, w^{\mu})$ and (u, v, w) in each of these directions, respectively. The large and small particles are assumed to have the same constant intrinsic density, $\rho^{l*} = \rho^{s*}$, and (1), (4) and (5) therefore imply that the bulk density ρ is also equal to the same constant value. It follows from the bulk mass balance that the bulk velocity field is incompressible

$$\frac{\partial u}{\partial x} + \frac{\partial v}{\partial y} + \frac{\partial w}{\partial z} = 0. \tag{6}$$

This is one of the key assumptions that is made in nearly all granular avalanche models [7, 25–37]. The other important assumption for compatibility with existing models, is that the bulk pressure p is lithostatic through the avalanche depth

$$p = \rho g(h - z)\cos\zeta, \tag{7}$$

which is true, provided the acceleration terms are negligible in the normal component of the bulk momentum balance.

During percolation the small grains can not support as much of the overburden pressure and the larger grains have to support proportionately more of the load. The driving force for particle size segregation are therefore perturbations to the lithostatic pressure distribution [16, 21, 22]. Instead of relating the partial pressure to the bulk pressure using a linear volume fraction dependent scaling, as in standard mixture theory, Gray and Thornton [21] introduced a linear scaling

$$p^{\mu} = f^{\mu} p, \quad \mu = l, s, \tag{8}$$

with a factor f^{μ} that could deviate away from ϕ^{μ}. The functions f^{μ} satisfy three constraints:-

$$\left.\begin{array}{lll} \text{(i)} & f^l + f^s = 1, & \\ \text{(ii)} & f^s = 1 \quad \text{when} & \phi^s = 1, \\ \text{(iii)} & f^l = 1 \quad \text{when} & \phi^l = 1, \end{array}\right\} \tag{9}$$

which ensure that the partial pressures sum to the bulk pressure (4), and that when either of the constituents are in a pure phase they carry all of the load. Although there are many functions that satisfy these constraints the simplest non-trivial functions are

$$f^l = \phi^l + b\phi^s\phi^l, \qquad f^s = \phi^s - b\phi^s\phi^l, \tag{10}$$

where b is the magnitude of the perturbation. To balance the pressure perturbations in the normal momentum balance equations (3), Gray and Thornton [21] and Thornton et al. [22] introduced an interaction drag $\mathbf{B}^{\mu}$ with a simple linear velocity dependent drag

$$\mathbf{B}^{\mu} = p\nabla f^{\mu} - \rho^{\mu} c(\mathbf{u}^{\mu} - \mathbf{u}) - \rho d\nabla\phi^{\mu}, \qquad \mu = l, s, \tag{11}$$

with drag coefficient c. Gray and Chugunov [16] introduced a further gradient dependent remixing force that drives the grains of phase μ towards areas of lower concentration. The strength of these diffusive forces is ρd. The interaction drag (11) automatically satisfies the constraint that $\mathbf{B}^l + \mathbf{B}^s = 0$, and when it is substituted into the constituent momentum balances the first term combines with the partial pressure gradient $-\nabla(f^{\mu}p)$ to leave $-f^{\mu}\nabla p$. Assuming that the acceleration terms are negligible, the normal component of the constituent momentum balances reduces to

$$\phi^{\mu} w^{\mu} = \phi^{\mu} w + (f^{\mu} - \phi^{\mu})(g/c)\cos\zeta - (d/c)\partial\phi^{\mu}/\partial z, \quad \mu = l, s. \tag{12}$$

Substituting for the pressure fluctuation functions (10) and dividing through by the volume fraction ϕ^{μ} implies that the normal velocities of the large and small particles are

$$w^l = w + q\phi^s - D\frac{\partial}{\partial z}(\ln\phi^l), \tag{13}$$

$$w^s = w - q\phi^l - D\frac{\partial}{\partial z}(\ln\phi^s), \tag{14}$$

where the maximum percolation velocity of the grains q and the diffusivity D are

$$q = (b/c)\, g \cos\zeta, \quad D = d/c. \tag{15}$$

Within the avalanche the segregation velocities $\mathbf{u}^\mu - \mathbf{u}$ are assumed to be of the same order of magnitude as the bulk normal velocity w, which is a lot less than the bulk down and cross slope velocities. It follows that to leading order the down and cross slope constituent velocities are equal to their bulk counterparts

$$u^\mu = u, \quad v^\mu = v, \quad \mu = l, s. \tag{16}$$

Substituting (13), (14) and (16) into the small particle mass balance (2) yields the segregation-remixing equation

$$\frac{\partial \phi^s}{\partial t} + \frac{\partial}{\partial x}(\phi^s u) + \frac{\partial}{\partial y}(\phi^s v) + \frac{\partial}{\partial z}(\phi^s w) - \frac{\partial}{\partial z}(q\phi^s \phi^l) = \frac{\partial}{\partial z}\left(D\frac{\partial \phi^s}{\partial z}\right). \tag{17}$$

The first four terms simply advect the local concentration with the bulk flow, the fifth is responsible for segregation and the sixth diffuses the small particles. The segregation-remixing equation (17) is parabolic for $D > 0$ and reduces to a hyperbolic equation when $D = 0$. The reduced model is termed the *hyperbolic segregation theory* or *segregation theory* for short. The segregation flux has the interesting property that it shuts off when the concentration of small particles equals zero or unity, so ϕ^s automatically stays in the range $[0,1]$.

In the absence of diffusion, equations (13)–(14) show that the large particles rise up until there are no more small particles, while small particles percolate downwards until there are no more coarse grains. This tends to drive the grains into completely separated *inversely graded layers* with all the large particles on top of the fines [1]. The hyperbolic segregation equation is related to the theory of sedimentation [38, 39] and is also very closely related to Savage and Lun [1]'s kinetic sieving and squeeze expulsion model. The link to Savage and Lun [1] is not immediately apparent, as they formulated their theory in terms of the layer number density ratio, η, and the particle diameter ratio, σ, instead of volume fractions. However, by substituting the definitions $\phi^l = 1/(1+\eta\sigma^3)$ and $\phi^s = \eta\sigma^3/(1+\eta\sigma^3)$ into their equations (6.4) and (6.3) we can see that the net percolation velocities have the same leading order concentration dependence as (13) and (14). Savage and Lun [1]'s information entropy approach yields considerably more structure for the segregation rate, but there is no dependence on gravity. The mixture approach does not provide as much structure for q, but it does have an explicit dependence on gravity in (15), which sets a direction for segregation and reflects the gravity driven nature of the kinetic sieving process. Thornton et al. [22] used ternary mixture theory to derive (17) in the presence of an interstitial fluid. This theory had an extra relative density difference factor $\hat{\rho}$ in q, which was able to explain the reduced segregation rates in liquid particle mixtures and the absence of segregation with a density matched fluid, observed in the experiments of Vallance and Savage [40].

The segregation-remixing equation (17) is closely related to Burgers' equation [41], and smoothes out the sharp concentration jumps that develop in the hyperbolic theory. Dolgunin and Ukolov [42] were the first to write down this form of the equation, by ingeniously spotting that the segregation flux must shut off when $\phi^s = 0, 1$, but there was no formal derivation. Khakhar et al. [43] went on to use equation (17) to study the equilibrium segregation of particles of different densities, but the same size, and obtained good agreement with experimental measurements in rotating drums. More recently, Gray and Chugunov [16] showed that steady-state solutions were in good agreement with particle dynamics simulations of chute flows of large and small particles of Khakhar et al. [44], which is reproduced in the bottom panel of figure 2. Both experiments and particle dynamics simulations [45, 46] are likely to be very useful in determining the functional dependence of q and D on other parameters, such as the shear rate, the particle-size ratio and the overburden pressure. An example of this is provided by Hajra and Khakhar [47] who used rotating drum experiments to infer that even small size differences are sufficient to cause segregation, but once the size ratio reaches a critical value the driving force for segregation saturates. It may also be possible to push bi-disperse kinetic theories [48–50] into the dense regime and find a link between the two approaches.

NON-DIMENSIONALIZATION, BOUNDARY AND JUMP CONDITIONS

Avalanches are shallow, with their typical thickness H being much less than their length L. The incompressibility condition (6) implies that, if typical down slope velocities are of magnitude U, then typical normal velocities are of magnitude HU/L. The variables are non-dimensionalized to reflect these scalings

$$(x,y,z) = L(\tilde{x},\tilde{y},\varepsilon\tilde{z}), \quad (u,v,w) = U(\tilde{u},\tilde{v},\varepsilon\tilde{w}), \quad t = (L/U)\tilde{t}, \tag{18}$$

where the tilde denotes a non-dimensional variable. Substituting these into (17) and dropping the tildes and the superscript s implies that the non-dimensional segregation-remixing equation is

$$\frac{\partial \phi}{\partial t} + \frac{\partial}{\partial x}(\phi u) + \frac{\partial}{\partial y}(\phi v) + \frac{\partial}{\partial z}(\phi w) - \frac{\partial}{\partial z}\Big(S_r \phi (1-\phi)\Big) = \frac{\partial}{\partial z}\left(D_r \frac{\partial \phi}{\partial z}\right), \tag{19}$$

where the non-dimensional segregation and diffusive-remixing numbers are

$$S_r = \frac{qL}{HU}, \quad \text{and} \quad D_r = \frac{DL}{H^2 U}, \tag{20}$$

respectively. Provided there is no erosion or deposition, there is no flux or large or small particles at the surface and basal boundaries of the avalanche. This can be expressed by the nonlinear boundary condition

$$S_r \phi (1-\phi) + D_r \frac{\partial \phi}{\partial z} = 0, \tag{21}$$

which insulates the avalanche from the exterior. In the hyperbolic theory shocks may also develop on a propagating surface of discontinuity across which a jump condition [51] must be satisfied

$$[\![\phi(\mathbf{u}\cdot\mathbf{n} - v_n)]\!] = [\![S_r \phi (1-\phi)\mathbf{k}\cdot\mathbf{n}]\!], \tag{22}$$

where the jump bracket $[\![f]\!] = f^+ - f^-$ is the difference of f evaluated on the forward "+" and rearward "-" side of the surface, $\mathbf{k}$ is the unit vector normal to the chute, $\mathbf{n}$ is the unit normal to the surface and v_n is it's normal speed. A Lax entropy condition implies that the shock will be stable if and only if the shock is inversely graded [52].

TIME-DEPENDENT SOLUTIONS OF THE SEGREGATION-REMIXING EQUATION

Gray and Chugunov [16] constructed a general time-dependent solution in a flow of unit depth with no down or cross slope gradients in concentration

$$u = u(z), \quad v = v(z), \quad w = 0, \quad \partial\phi/\partial x = 0, \quad \partial\phi/\partial y = 0, \quad O < z < 1. \tag{23}$$

In this case the segregation-remixing equation (19) reduces to

$$\frac{\partial \phi}{\partial t} - \frac{\partial}{\partial z}\Big(S_r \phi (1-\phi)\Big) = D_r \frac{\partial^2 \phi}{\partial z^2}, \tag{24}$$

which is subject to the surface and basal boundary conditions (21) and the initial condition

$$t = 0: \qquad \phi = \phi_i(z), \tag{25}$$

which must be independent of x and y. The reduced segregation-remixing equation can be mapped directly on to Burgers equation, which can in turn be linearized by using the Cole-Hopf transformation [53, 54]. Gray and Chugunov [16] used this sequence of transformations to linearize both the segregation-remixing equation (24) and the nonlinear boundary conditions (21). The resulting diffusion problem was then solved by using Fourier series. The general solution takes the form

$$\phi = \frac{1}{2}\Big(1 - \frac{2z_0}{\omega}\frac{\partial \omega}{\partial z}\Big), \tag{26}$$

where the segregation-remixing length scale $z_0 = D_r/S_r$. Considerable simplification is achieved by splitting the solution ω into a steady-state and time dependent part

$$\omega = \omega_s + \omega_t, \tag{27}$$

where

$$\omega_s = \chi(1)\frac{\sinh(z/(2z_0))}{\sinh(1/(2z_0))} - \frac{\sinh((z-1)/(2z_0))}{\sinh(1/(2z_0))}, \tag{28}$$

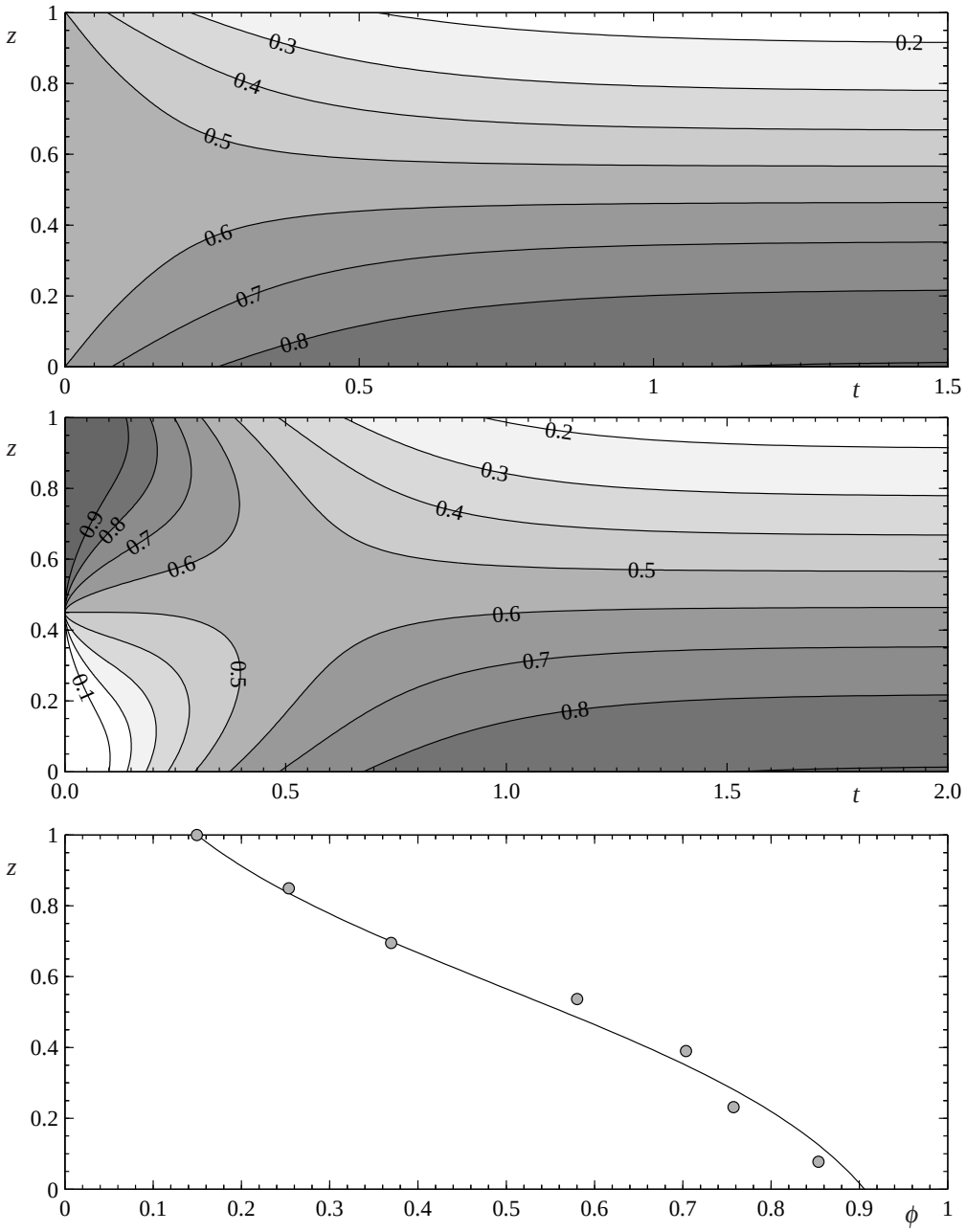

FIGURE 2. The upper and middle panels show two contour plots of the evolution of the the small particle concentration through the depth of the avalanche for $S_r = 1$ and $D_r = 0.25$. In the top panel the avalanche is initially homogeneously mixed with an initial concentration $\phi_0 = 0.55$ and in the middle panel the small grains are initially on top of the large ones and are separated by a sharp interface at $z_r = 0.45$. For these parameters the same steady-state develops, which is shown in the bottom panel as a profile of the small particle concentration ϕ with depth. The dots are the equivalent steady state concentrations derived from the particle dynamics simulations of Khakhar et al. [44] for comparison.

$$\omega_t = \sum_{n=1}^{\infty} A_n \exp\left(-\left(\frac{1}{4} + n^2\pi^2 z_0^2\right)\frac{S_r t}{z_0}\right)\sin(n\pi z)\,. \tag{29}$$

The function χ is defined as

$$\chi(z) = \exp\left(-\int_0^z \frac{2\phi_i - 1}{2z_0}\,dz'\right), \quad \text{and} \quad \chi(1) = \exp\left(-\int_0^1 \frac{2\phi_i - 1}{2z_0}\,dz'\right), \tag{30}$$

which are both dependent on the initial concentration profile $\phi_i(z)$ and the segregation-remixing length z_0. At $t = 0$ equation (29) reduces to a Fourier Sine series for ω_t and the coefficients A_n can be determined by integration in the usual way. The coefficient A_n can be split into two parts, $A_n = B_n - C_n$, where B_n is given by an integral of the transformed initial conditions, $\chi(z)$, and C_n is dependent on an integral of the steady-state solution ω_s. It follows that to construct a specific solution it is necessary to compute

$$B_n = 2\int_0^1 \chi(z)\sin(n\pi z)\,dz, \quad C_n = \frac{8n\pi z_0^2}{1 + 4n^2\pi^2 z_0^2}\Big(1 - (-1)^n\chi(1)\Big), \tag{31}$$

where the integral for C_n has already been evaluated by substituting the steady-state solution (28).

Two different initial conditions are shown in figure 2. In the top panel the grains are initially homogeneously mixed with concentration $\phi_0 = 0.55$. As time progresses the small particles percolate down towards the base of the avalanche and the large particles are pushed upwards until a balance establishes itself with the diffusive effects of remixing. For large time the concentration profile therefore approaches an inversely graded steady state, which is shown in the bottom panel of figure 2. The grey circles are points derived from the steady-state particle dynamics simulations of Khakhar et al. [44], which the theory fits well for $S_r = 1$ and $D_r = 0.25$, giving a segregation-remixing length $z_0 = D_r/S_r = 0.25$. The middle panel shows the solution for an unstably stratified initial distribution, with all the small particles above the large ones, separated by a discontinuity at height $z_r = 0.45$. The initial discontinuity is rapidly smoothed out by diffusion, before percolation and squeeze expulsion take over as the dominant means of transport. The small particles percolate down from the top and collect at the base, while the large ones rise from the base to the surface, until the same steady-state distribution as the top and bottom panels is established.

STEADY STATE SOLUTIONS TO THE SEGREGATION EQUATION

In the last section we showed that segregation-remixing theory is able to reproduce steady state one-dimensional profiles produced by particle dynamics simulations, which lends considerable weight to this approach. The chute flow experiments of Savage and Lun [1] suggest that when strongly stratified layers develop the diffusive term in (19) can be neglected. It is therefore of interest to study the hyperbolic segregation equation, which allows complicated physical problems to be treated in a simple way and gives considerable insight into the nature of segregation in granular avalanches. In a steady uniform avalanche of unit depth

$$u = u(z) \geq 0, \quad v = 0, \quad w = 0, \quad \text{in} \quad 0 < z < 1, \quad x > 0, \tag{32}$$

the steady hyperbolic segregation equation (19) and the no flux condition (21) reduce to

$$\frac{\partial}{\partial x}(\phi u) - \frac{\partial}{\partial z}\Big(S_r\phi(1-\phi)\Big) = 0, \tag{33}$$

$$\phi(1-\phi) = 0, \quad \text{at} \quad z = 0, 1. \tag{34}$$

This can be written as a first order quasi-linear equation by expanding out the derivatives

$$u\frac{\partial\phi}{\partial x} + S_r(2\phi - 1)\frac{\partial\phi}{\partial z} = 0, \tag{35}$$

and solved by the method of characteristics. The small particle concentration is equal to a constant ϕ_λ along the characteristic curve given by

$$u\frac{dz}{dx} = S_r(2\phi_\lambda - 1). \tag{36}$$

Solutions for general velocity fields can be constructed by defining a depth-integrated velocity coordinate

$$\psi = \int_0^z u(z')\,\mathrm{d}z', \tag{37}$$

that increases monotonically with z. By virtue of the scalings (18), we may assume without loss of generality that at the free surface $\psi(1) = 1$. The mapping (37) transforms (36) into a linear equation

$$\frac{d\psi}{dx} = S_r(2\phi_\lambda - 1), \tag{38}$$

which can be integrated, subject to the initial condition that the characteristic starts at $(x_\lambda, \psi_\lambda)$, to give a straight line

$$\psi = \psi_\lambda + S_r(2\phi_\lambda - 1)(x - x_\lambda). \tag{39}$$

The position in physical space can be calculated by inverting the transformation (37) once $u(z)$ is prescribed. The beauty of the depth-integrated velocity coordinates is that the solutions constructed with it are valid for all velocity fields provided the inverse mapping is well defined. In this paper, we will consider linear velocity profiles

$$u = \alpha + 2(1-\alpha)z, \quad 0 \le \alpha \le 1, \tag{40}$$

which include plug flow ($\alpha = 1$), simple shear ($\alpha = 0$) and shear with basal slip, for intermediate values of α. The integral (37) implies that the depth-integrated velocity coordinate

$$\psi = \alpha z + (1-\alpha)z^2, \tag{41}$$

which is quadratic and can be inverted to give

$$z = \begin{cases} \psi, & \alpha = 1, \\ \dfrac{-\alpha + \sqrt{\alpha^2 + 4(1-\alpha)\psi}}{2(1-\alpha)}, & \alpha \neq 1. \end{cases} \tag{42}$$

Homogeneous inflow

Gray and Thornton [21] considered the case in which there is an inflow at $x = 0$ at which the particles enter in a homogeneously mixed state with concentration

$$\phi = \phi_0, \qquad \text{at} \qquad x = 0, \quad 0 < z < 1. \tag{43}$$

Through most of the avalanche the inflow concentration ϕ_0 is simply swept into the domain by the characteristics, and the small particles percolate downwards by kinetic sieving and the large grains are squeezed upwards. At the base, however, the no flux condition (34) implies that there are no more large particles to rise up, and instead the small particles separate out across a concentration shock. In the uniform flow field (32) the jump condition (22) reduces to

$$\left[\!\left[\phi u \frac{dz}{dx} + S_r \phi(1-\phi) \right]\!\right] = 0, \tag{44}$$

provided the shock is stationary, $v_n = 0$. Dividing both sides by $[\![\phi]\!]$ yields

$$u\frac{dz}{dx} = S_r(\phi^+ + \phi^- - 1), \tag{45}$$

where ϕ^+ and ϕ^- are the values of the concentration on the forward and rearward sides of the discontinuity. Using the mapping (37) this reduces to

$$\frac{d\psi}{dx} = S_r(\phi^+ + \phi^- - 1). \tag{46}$$

The position of the bottom shock, which separates the fines from the homogeneous mixture, can be computed from (46) by substituting $\phi^- = \phi_0$ and $\phi^+ = 1$ and integrating, subject to the boundary condition that $\psi = 0$ at $x = 0$, to give

$$\psi_{bottom} = S_r \phi_0 x. \tag{47}$$

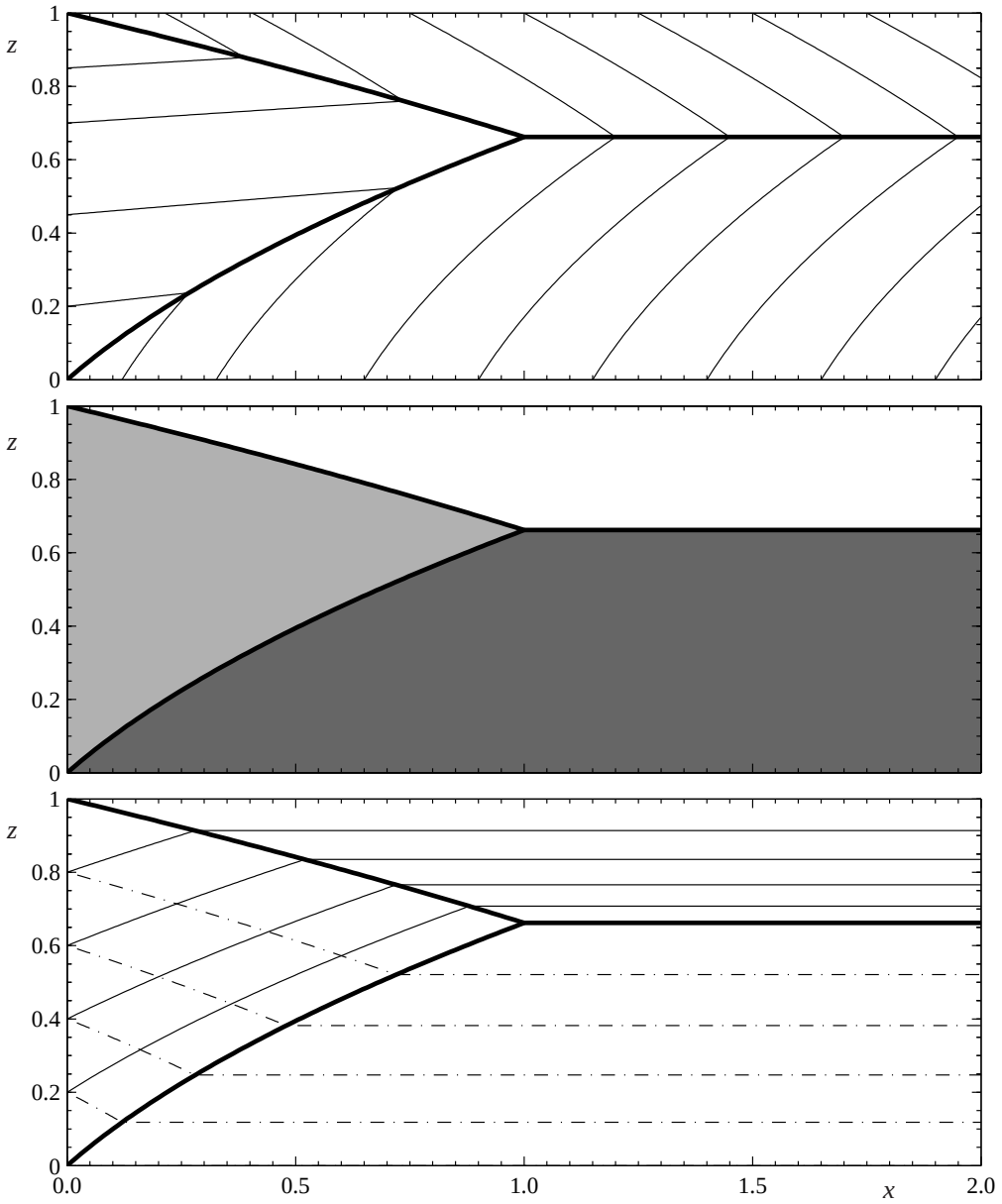

FIGURE 3. The steady-state segregation solution for a homogeneous inflow of concentration $\phi_0 = 0.55$ at $x = 0$ in a unit thickness avalanche with a linear shear profile through its depth ($\alpha = 0.5$) and the non-dimensional segregation number $Sr = 1$. The top panel shows the shocks as thick solid lines and the characteristics as thin lines. The middle panel indicates the concentration, with the white area composed of all large particles, the dark grey area of all fines and the light grey region being at the inflow concentration. The bottom panel shows the large particle paths with thin solid lines and the small particle paths with thin dot-dash lines.

The basal layer of small particles therefore becomes progressively thicker with increasing downstream distance. A similar thing happens at the top of the avalanche, where the boundary condition (34) implies that there are no more small particles to percolate downwards, and the large grains separate out into a pure phase across a shock. Substituting $\phi^+ = 0$ and $\phi^- = \phi_0$ into (46) and integrating subject to the boundary condition $\psi = 1$ at $x = 0$, implies that the top shock

$$\psi_{top} = 1 - S_r(1 - \phi_0)x. \tag{48}$$

The top layer of large particles also becomes thicker with increasing x, and the top and bottom shocks meet to form a triple-point at $x_{triple} = 1/S_r$, $\psi_{triple} = \phi_0$. Downstream of x_{triple} a third shock is formed that separates a pure layer of

large particles from a pure layer of fines below. Substituting $\phi^+ = 0$ and $\phi^- = 1$ into (46) and integrating implies that the shock separating the inversely graded layers is at constant height

$$\psi_{inverse} = \phi_0, \quad \text{for} \quad x \geq x_{triple}. \tag{49}$$

The solution therefore consists of three shocks that separate regions of homogeneously mixed material (light grey) adjacent to the inflow, from small particles (dark grey) next to the base and large particles (white) at the surface of the avalanche, as illustrated in the middle panel of figure 3. The top panel shows how each shock (thick line) has characteristics (thin lines) intersecting from both sides, which is required by the entropy condition. This problem is the hyperbolic counterpart of the time-dependent segregation remixing problem shown in the top panel of figure 2. The key differences are that (i) x replaces t along the lower axis, (ii) there are sharp shocks instead of a smooth transition to a diffuse steady-state and (iii) the inversely graded layer of large particles at the surface is thinner than would develop in the equivalent time-dependent problem, because there is a higher mass flux near the surface.

Particle paths of the large and small grains

One of the major benefits of using the hyperbolic model is that it is possible to exactly reconstruct the large and small particle paths. They satisfy the equations

$$\frac{dx^\mu}{dt} = u^\mu, \quad \frac{dz^\mu}{dt} = w^\mu, \qquad \mu = l, s \tag{50}$$

with the non-dimensional forms of the constituent velocities (13), (14) and (16) are given by

$$u^l = u, \quad w^l = w + S_r\phi, \quad u^s = u, \quad w^s = w - S_r(1-\phi). \tag{51}$$

Using the chain rule and the depth-integrated velocity coordinate transformation

$$\frac{d\psi^l}{dx} = S_r\phi, \quad \frac{d\psi^s}{dx} = -S_r(1-\phi). \tag{52}$$

For the homogeneously mixed inflow problem discussed above, the small particles enter at $x = 0$ at a height ψ^s_{enter} and percolate downwards along the path

$$\psi^s = \psi^s_{enter} - S_r(1-\phi_0)x, \tag{53}$$

until they hit the bottom shock at $x^s_{cross} = \psi^s_{enter}/S_r$ and then move parallel to the base

$$\psi^s = \phi_0\psi^s_{enter}, \quad x > x^s_{cross}, \tag{54}$$

through a region of pure fines. Conversely large particles entering at height ψ^l_{enter} are pushed upwards, by squeeze expulsion, along the path

$$\psi^l = \psi^l_{enter} + S_r\phi_0 x, \tag{55}$$

until they reach the top shock at $x^l_{cross} = (1-\psi^l_{enter})/S_r$, after which they move downslope at height

$$\psi^l = 1 - (1-\phi_0)(1-\psi^l_{enter}), \quad x > x^l_{cross}, \tag{56}$$

through a region of purely large grains. The particle paths are illustrated in the bottom panel of figure 3 using solid lines for the large particle paths and dot-dash lines for the fines. From this we see that the top shock is also a small particle path, while the bottom shock is also a large particle path. This can also be proved by observing that the shock condition (46) degenerates to the particle path equations (52) when ϕ^+ is equal to zero or unity.

Unstably stratified inflow

Thornton et al. [22] investigated the case on an unstably stratified inflow in which all the small particles are fed into the chute above the large particles

$$\phi = \begin{cases} 1 & z_r \leq z \leq 1, \\ 0 & 0 \leq z < z_r. \end{cases} \tag{57}$$

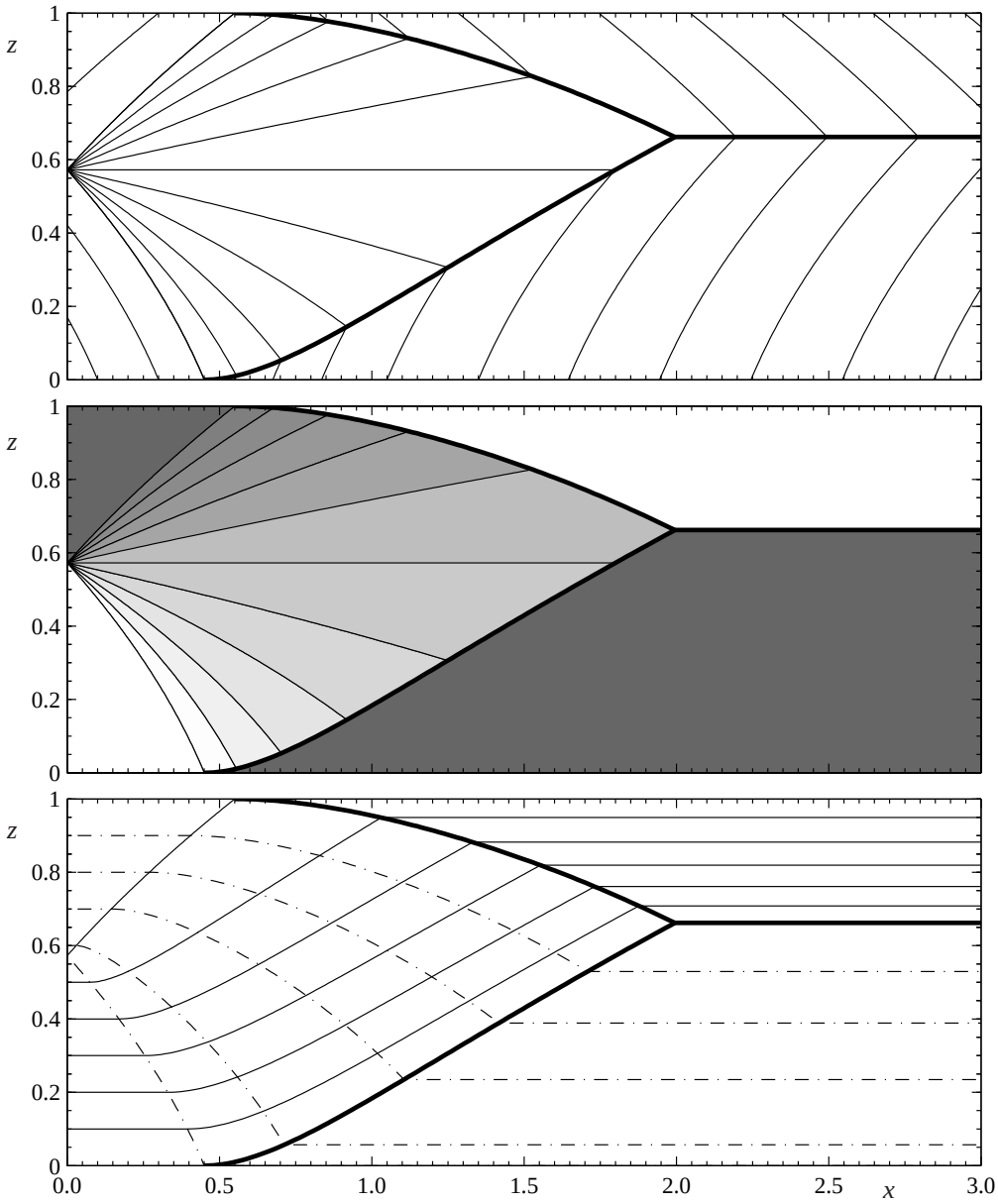

FIGURE 4. The steady-state segregation solution for in flow at $x = 0$, where a layer of small particles enters on top of a layer of coarse grains. The interface between the two layers lies at a height $z_r = 0.5724$. The avalanche is assumed to be of unit thickness with a linear shear profile through its depth ($\alpha = 0.5$) and the non-dimensional segregation number $S_r = 1$. The top panel shows the shocks as thick solid lines and the characteristics as thin lines. The middle panel indicates the concentration, with the white area composed of all large particles, the dark grey area of all fines, and the fan shown with contours of 0.1 unit intervals. The bottom panel shows the large particle paths with thin solid lines and the small particle paths with thin dot-dash lines. The inversely graded steady-state shock height is the same as in figure 3.

One possible solution that satisfies the shock condition (46), is simply to continue the discontinuity at height z_r down the chute. However, this is not admissible, because it does not satisfy the Lax entropy condition [52], which requires that the grains must be inversely graded across the shock. Instead a rarefaction fan is formed, which is centred at $(0, z_r)$. In depth averaged velocity coordinates (37) this corresponds to the position $(0, \psi_r)$, and the characteristic equation (39)

then implies that the concentration within the fan is given by

$$\phi = \frac{1}{2}\left(1 + \frac{\psi - \psi_r}{S_r x}\right), \quad |\psi - \psi_r| < S_r x, \tag{58}$$

which is shown in the top panel of figure 4. The lowest characteristic that emanates from the fan has concentration $\phi = 0$. It intersects with the base of the flow at $x_b = \psi_r / S_r$ and represents the first small particle to percolate down to the base of the flow. As in the homogeneous problem, there is no flux of large particles across the basal boundary, and so the small grains separate out into a pure phase across a concentration shock that emanates from $(x_b, 0)$. The shock height can be found by integrating the linear ordinary differential equation that is obtained by substituting the fan concentration (58) and the small particle concentration into the shock condition (46). This implies that the basal shock

$$\psi_{bottom} = \psi_r + S_r x - 2\sqrt{S_r \psi_r x}. \tag{59}$$

Similarly, the first large particle reaches the surface at $x_s = (1 - \psi_r)/S_r$ and the large particles then begin to separate out into a pure phase across a concentration shock that emanates from $(x_s, 1)$. Solving the shock condition (46) with the expansion fan (58) on one side and large particles on the other, yields an equation for the top shock

$$\psi_{top} = \psi_r - S_r x + 2\sqrt{S_r(1 - \psi_r)x}. \tag{60}$$

The top and bottom shocks meet at the triple point

$$x_{triple} = \frac{1}{S_r}\left(\sqrt{\psi_r} + \sqrt{1 - \psi_r}\right)^2, \qquad \psi_{triple} = 1 - \psi_r, \tag{61}$$

and a third shock is formed that separates the inversely graded layers of large and small particles. The shock condition (46) implies that this is parallel to the base of the flow at height

$$\psi_{inverse} = \psi_{triple}, \qquad x \geq x_{triple}, \tag{62}$$

which now satisfies the Lax entropy condition [52]. The expansion fan and the three shocks are shown in figure 4. The top panel shows the characteristics, which intersect either side of the shocks, and the centre panel shows the concentration using a grey scale. This solution shows how an unstably stratified inflow readjusts into a stable configuration. Small particles that enter near the surface of the avalanche, move straight downslope until they reach the expansion fan. Here they percolate downwards, until they cross the bottom shock and enter into a pure phase of small particles again implying that they move straight downslope again, but at a much lower level than they started. The small particle paths are shown as dot-dash lines in the bottom panel of figure 4. Conversely large particles entering near the bottom of the flow, move straight downslope until they reach the expansion fan. They are then squeezed upwards until they reach the top shock, after which they move straight downslope again, but at a much higher position than where they started. The detailed formulae of the particle paths can be found in Thornton et al. [22].

BREAKING SIZE SEGREGATION WAVES

Gray et al. [55] and Shearer et al. [52] have gone on to construct fully time and spatially dependent two-dimensional solutions to the segregation equation. These solutions show that inversely graded shocks can develop which have monotonically decreasing sections. As these are transported downstream the velocity shear causes the interface to steepen and it eventually breaks, as small particles are sheared over the top of large grains. Thornton and Gray [56] used shock capturing numerical simulations to show that these breaking waves precess like a spinning rugby ball and move downstream at approximately constant speed. The time-dependent behaviour of these lens-like features is extremely complicated [57], but eventually they settle down towards a steady travelling wave.

An exact solution for the breaking wave [56] can be constructed by transforming equation (19) into a frame

$$\xi = x - u_{lens} t, \tag{63}$$

which moves downslope at speed u_{lens}. The steady-state segregation equation in the moving frame is then

$$\frac{\partial}{\partial \xi}\Big(\phi(u - u_{lens})\Big) - \frac{\partial}{\partial z}\Big(S_r \phi(1 - \phi)\Big) = 0, \tag{64}$$

which has the same form as (33) with a redefined velocity field. Defining a depth-integrated velocity coordinate

$$\psi(z) = \int_0^z u(z') - u_{lens} \mathrm{d}z', \tag{65}$$

the method of characteristics again implies that the concentration is equal to ϕ_λ along the straight line

$$\psi = \psi_\lambda + S_r(2\phi_\lambda - 1)(\xi - \xi_\lambda), \tag{66}$$

emanating from $(\xi_\lambda, \psi_\lambda)$ in mapped coordinates. The shock condition (22) transforms to

$$\frac{d\psi}{d\xi} = S_r(\phi^+ + \phi^- - 1). \tag{67}$$

Equations (66) and (67) are the direct equivalents to equations (39) and (46) in the fixed domain.

Consider a unit depth avalanche that is inversely graded up slope of a breaking wave and has a region of purely large particles downstream of it. The inversely graded shock is assumed to lie at a height $z_{inverse}$ as shown in figure 5. The breaking size segregation wave has the property that there is no net flux of small particles across the wave. This can be expressed by the integral

$$\int_0^{z_{inverse}} \phi(u - u_{lens}) \mathrm{d}z = 0. \tag{68}$$

Using the linear velocity field defined in (40) this implies that the speed of the lens is equal to

$$u_{lens} = \alpha + (1 - \alpha) z_{inverse}. \tag{69}$$

The depth-integrated velocity coordinate (65) then becomes

$$\psi = (1 - \alpha) z (z - z_{inverse}), \tag{70}$$

which is zero at $z = 0$ and $z = z_{inverse}$, and attains a minimum, $\psi_{lens} = -\frac{1}{4}(1 - \alpha) z_{inverse}^2$ at height $z_{lens} = z_{inverse}/2$. This height is special, because it is also the height at which there is no net velocity relative to the lens, i.e. $u(z_{lens}) = u_{lens}$. The height z_{lens} is shown as a dotted line in the top panel of figure 5. Particles above z_{lens} move downslope faster than the breaking wave, while grains below z_{lens} move downslope slower then the lens and are overtaken by it. In the moving frame, particles therefore move from left to right above the dotted line and from right to left below it.

The solution starts by assuming that there is an expansion fan, centred on the no mean flow line $\psi = \psi_{lens}$ at an arbitrary downstream position ξ_A, within which the concentration is

$$\phi_{top} = \frac{1}{2}\left(1 + \frac{\psi - \psi_{lens}}{S_r(\xi - \xi_A)}\right). \tag{71}$$

The fan is shown in the top panel of figure 5 emanating from point A. The characteristics for $\phi \in [1/2, 1]$ propagate upwards above the no mean flow line, and the $\phi = 1$ characteristic reaches the inversely graded shock at height $z_{inverse}$ when $\psi = 0$ at point B, which lies at $\xi_B = \xi_A - \psi_{lens}/S_r$. Here there are no more small particles to percolate downwards and the large grains separate out into a pure phase across a concentration shock. Substituting the fan concentration (71) and the large particle concentration into the shock condition (67) and integrating, subject to the condition that the shock starts at $(\xi_B, 0)$ in mapped coordinates, implies that the top shock

$$\psi_{top} = \psi_{lens} - S_r(\xi - \xi_A) + 2\sqrt{-\psi_{lens}}\sqrt{S_r(\xi - \xi_A)}, \tag{72}$$

where the constant $\sqrt{-\psi_{lens}}$ is real. The shock satisfies the Lax entropy condition because the concentration is inversely graded across it, and propagates down until it reaches the no mean flow line $\psi = \psi_{lens}$ at point C. This is the furthest downstream distance of the lens and has position $\xi_C = \xi_A - 4\psi_{lens}/S_r$. The shock (72) could be continued down into the lower domain, but because the flow changes direction this would imply that a pure region of large particles would lie beneath a region of mixed particles. This configuration is not inversely graded and the shock is therefore not admissible by the Lax entropy condition [52]. Instead a lower expansion fan forms, that is centred at (ξ_C, ψ_{lens}), and within which the concentration is

$$\phi_{bottom} = \frac{1}{2}\left(1 - \frac{\psi - \psi_{lens}}{S_r(\xi_C - \xi)}\right). \tag{73}$$

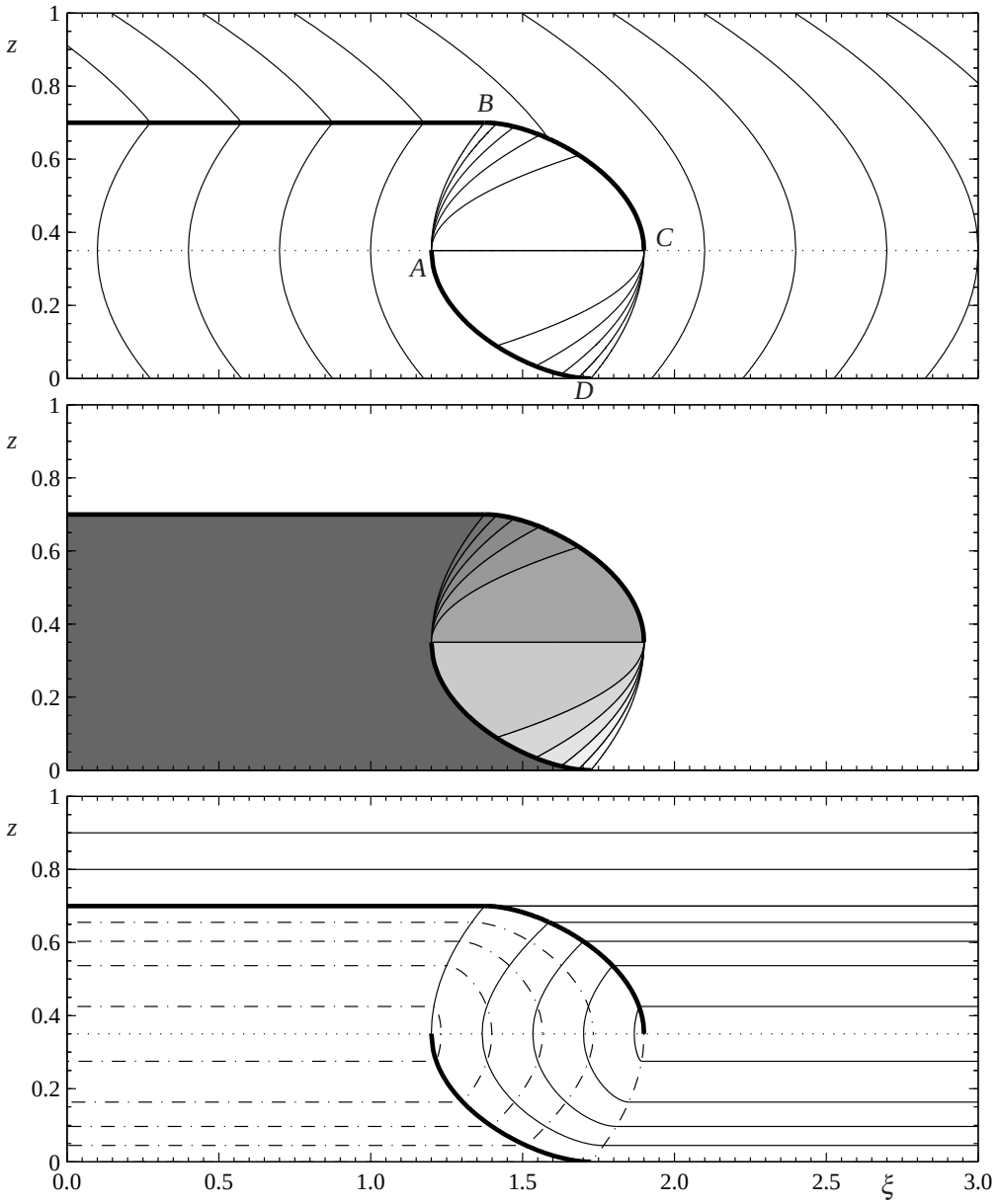

FIGURE 5. A breaking size segregation wave connects an upstream inversely graded avalanche from a downstream region of purely large grains. The height of the inversely graded interface $z_{inverse} = 0.7$, there is a linear velocity profile through the avalanche depth with $\alpha = 0.5$ and $S_r = 0.35$. In the top panel expansion fans are centred at points A and C and the shocks are shown with thick solid lines. The thin lines are characteristics, which change direction at the no mean flow line, which is marked by a dotted line. In the middle panel the concentration is shown using a contour scale with 0.1 unit intervals. Darker regions correspond to greater concentrations of fines and the the white region is composed of large particles. In the bottom panel the particle paths are shown in the moving frame ξ. Large particle paths are shown with solid lines and small particle paths with dot-dash lines.

This matches up with the upper expansion fan (71) centred at point *A*, since the concentration is equal to 1/2 in both cases on the no mean flow line $\psi = \psi_{lens}$. The characteristics emanating from point C lie in the range $\phi \in [0, 1/2]$ and curve downwards and backwards in the moving frame. The outermost, $\phi = 0$, characteristic hits the base of the avalanche at $\psi = 0$ at point *D*, which has position $\xi_D = \xi_C + \psi_{lens}/S_r$. Here there are no more large particles to be squeezed upwards and the small particles therefore separate out across a concentration shock. Solving the shock condition (67), with small particles on one side and the expansion fan (73) on the other, and, subject to the boundary

condition that the shock starts from $(\xi_D, 0)$, implies that the bottom shock

$$\psi_{bottom} = \psi_{lens} - S_r(\xi_C - \xi) + 2\sqrt{-\psi_{lens}}\sqrt{S_r(\xi_C - \xi)}. \tag{74}$$

This reaches the zero mean flow line, $\psi = \psi_{lens}$, at $\xi = \xi_C + 4\psi_{lens}/S_r = \xi_A$, which is the same as point A. The Lax entropy condition [52] predicts that a continuation of the lower shock is not admissible and it is instead replaced by an expansion fan centred at (ξ_A, ψ_{lens}), justifying the original assumption (71). The solution is now complete and is illustrated using a contour scale in the central panel of figure 5. It consists of two shocks, (72) and (74), and two expansion fans, (71) and (73), that are arranged in a 'lens'-like structure that propagates downstream with speed u_{lens} given by (69). These breaking size segregation waves are a very important feature of granular avalanches, because they allow particles to circulate in the flow. Thornton and Gray [56] have used equations (50) to reconstruct the large and small particle paths, which are illustrated in the bottom panel of figure 5. Large particles below the no mean flow line are caught up by the lens, rise up through it and exit into faster moving regions of the flow. While small particles that are above the no mean flow line catch up with the lens, percolate downwards and exit into a basal layer that is moving slower than the lens. In the example in figure 5 all the small particles are recirculated. While large particles below z_{lens} are recirculated between z_{lens} and $z_{inverse}$, and large particles above $z_{inverse}$ simply move downstream faster than the breaking wave.

PARTICLE SIZE SEGREGATION AT BOULDERY FLOW FRONTS

Gray and Ancey [5] observed that coarse particle rich flow fronts form in small scale stratification experiments [15, 19, 20, 58, 59] performed in a two-dimensional Hele-Shaw cell with a 3mm gap. A particularly interesting feature of these flows was that the coarse rich front remained at almost constant length [5], with those large grains that reached it, being deposited to form a carpet of grains over which the rest of the avalanche flowed. This can be seen in figure 5, where the large particles that form the current avalanche, or have just been deposited by it, are highlighted in white. The large rich flow front is connected to a small particle sandwich in the interior, with a layer of inversely graded large particles on top, and a static carpet of deposited large grains at the base. The stratification experiments of Gray and Ancey [5] are very closely analogous to self-channelizing flows, since large particles that reach the front are removed, by basal deposition in two-dimensions and lateral transport in three-dimensions, allowing the more mobile interior to continue to propagate downslope.

Gray and Ancey [5]'s observations allowed them to construct a travelling wave solution for the particle size distribution at the flow front by switching to a frame (ξ, z) moving downslope at the speed of the front u_F. Introducing the transformation

$$\xi = x - u_F t, \quad \tau = t, \tag{75}$$

the depth-integrated mass balance, the segregation equation (19) and the basal kinematic condition [see e.g. 5, 60], for a steady-state solution in the moving frame, become

$$\frac{\partial}{\partial \xi}\big(h(\bar{u} - u_F)\big) = -d, \tag{76}$$

$$\frac{\partial}{\partial \xi}\Big(\phi(u - u_F)\Big) + \frac{\partial}{\partial z}\Big(\phi w - S_r\phi(1-\phi)\Big) = 0, \tag{77}$$

$$(u_b - u_F)\frac{\partial b}{\partial \xi} - w_b = d, \tag{78}$$

where h is the avalanche thickness, b is the height of the basal deposit and d is the deposition rate. The basal velocity components u_b and w_b are assumed to be zero, which implies that $d = -u_F \partial b/\partial \xi$. Substituting this into (76) allows the depth-averaged mass balance equation to be integrated, subject to the condition that the flow front is located at $\xi = 0$, to show that

$$b = \lambda h, \quad \text{where} \quad \lambda = \frac{\bar{u} - u_F}{u_F}. \tag{79}$$

In order to close the model Gray and Ancey [5] assumed that $\bar{u}$ was equal to a constant throughout the flow. It follows the basal deposit height b is linearly related to the avalanche thickness h by the parameter λ and the constant depth-averaged velocity

$$\bar{u} = (1 + \lambda)u_F. \tag{80}$$

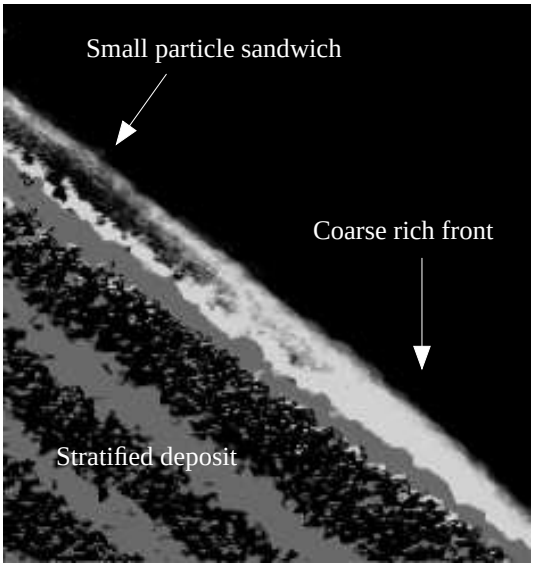

FIGURE 6. A composite image of the stratification pattern experiments of Gray and Ancey [5] that highlights the grains that are part of, or, have just been laid down by, the current avalanche. The flow front is almost entirely composed of large white sugar particles (500–600 μm), but behind it the active region has a layer of small dark iron spheres (210–420 μm) that are sandwiched between recently deposited large grains at the base and inversely graded large grains at the surface. The grains in the static stratified deposit that have been darkened, so that the large particles appear dark grey in colour. A complete sequence of stills can be found in Gray and Ancey [5] together with an animation of the flow in the online version of their paper.

Gray and Ancey [5] used the depth-averaged momentum balance to compute an exact solution for the avalanche thickness using Pouliquen and Forterre [61]'s basal friction law for rough beds. Here $h = h(\xi)$ is given. The downslope velocity is assumed to be linear with no slip at the base

$$u = \begin{cases} 2\overline{u}\left(\dfrac{z-b}{h}\right), & b \le z \le b+h, \\ 0, & 0 \le z < b, \end{cases} \tag{81}$$

and the incompressibility condition (6) then implies that the normal velocity

$$w = \begin{cases} \dfrac{\overline{u}}{h^2}\dfrac{dh}{d\xi}(z^2-b^2), & b \le z \le b+h, \\ 0, & 0 \le z < b. \end{cases} \tag{82}$$

In two-dimensions the depth-integrated velocity coordinate

$$\psi = \int_0^z u(\xi, z') - u_F \, dz', \tag{83}$$

is equivalent to the stream-function, since $\partial\psi/\partial z = u - u_F$ and $\partial\psi/\partial\xi = -w$. For the downslope velocity field defined in (81) this implies that

$$\psi = \begin{cases} \dfrac{\overline{u}}{h}(z-b)^2 - u_F z, & b \le z \le b+h, \\ -u_F z, & 0 \le z < b, \end{cases} \tag{84}$$

which is zero along the free-surface $z = b+h$ and the inclined base $z = 0$. Since the flow is steady, bulk particle paths are equal to lines of constant ψ. These are illustrated in the top panel of figure 7 using solid lines for paths that are deposited and dashed lines for those that are recirculated within the avalanche. The dotted line is the height $z_{u_F} = b + u_F h/(2\overline{u})$ where the velocity is equal to the front velocity, i.e. $u(z_{u_F}) = u_F$. Above the no mean flow line the bulk flow is from left to right, and below it is from right to left. The line also marks a local minimum in the stream-function coordinate $\psi_{u_F} = -u_F^2 h/(4\overline{u}) - u_F b$.

The stream-function coordinates are very useful for solving the segregation equation (77). Using incompressibility the segregation equation can be written in the quasi-linear form

$$(u-u_F)\frac{\partial \phi}{\partial \xi}+\Big(w+S_r(2\phi-1)\Big)\frac{\partial \phi}{\partial z}=0, \tag{85}$$

and the method of characteristics then implies that the concentration is equal to a constant value ϕ_λ along the characteristic curve $z=z(\xi)$ given by

$$(u-u_F)\frac{dz}{d\xi}-w=S_r(2\phi_\lambda-1). \tag{86}$$

When $z=z(\xi)$ differentiating the stream-function ψ with respect to ξ, using Leibniz's rule [62] and the incompressibility condition (6), yields the important identity

$$\frac{d\psi}{d\xi}=(u-u_F)\frac{dz}{d\xi}-w. \tag{87}$$

which linearizes the characteristic equation (86). Solving for the characteristic starting from $(\xi_\lambda,\psi_\lambda)$ therefore yields a straight line

$$\psi=\psi_\lambda+S_r(2\phi_\lambda-1)(\xi-\xi_\lambda), \tag{88}$$

in streamfunction coordinates. The identity (87) can also be used to show that the large and small particle paths (50) and the shock condition (22) also reduce to the familiar forms

$$\frac{d\psi^l}{d\xi}=S_r\phi, \qquad \frac{d\psi^s}{d\xi}=-S_r(1-\phi), \qquad \frac{d\psi}{d\xi}=S_r(\phi^+ +\phi^- -1), \tag{89}$$

respectively, even in the case of two-dimensional velocity fields. It is useful to note that the equation for the large particle path is identical to the equation for a shock condition when $\phi^+=1$. While, the small particle path equation is equivalent to the shock condition with $\phi^+=0$. Tracking large particles is therefore equivalent to solving for a shock with small particles on the forward side and tracking small particles is equivalent to solving for a shock with large particles on the other side.

Steady travelling wave solutions in a depositing flow field, only exist if all the large particles that reach the flow front are deposited. This necessarily implies that if the particles are inversely graded in the interior of the avalanche, the interface, ψ_L which lies along a bulk streamline, must lie in the region of those paths that are deposited, which are denoted by solid lines in the top panel of figure 7. Assuming that this is the case, the solution is very similar to the breaking wave solution of the previous section. There is an expansion fan centred at point A, which lies on the no mean flow line $\psi=\psi_{u_F}$. This expands into the upper domain of material moving towards the flow front and the concentration within the fan is

$$\phi_{top}=\frac{1}{2}\left(1+\frac{\psi-\psi_A}{S_r(\xi-\xi_A)}\right), \tag{90}$$

where (ξ_A,ψ_A) is the position of point A in stream-function coordinates. The leading $\phi=1$ characteristic AB intersects with the inversely graded layer $\psi=\psi_L$ at point B, which coordinates $\xi_B=\xi_A+(\psi_L-\psi_A)/S_r$. Since there are no more small particles above ψ_L to percolate downwards, a shock BC is generated between the expansion fan (90) on one side and a pure phase of large particles on the other. Solving the jump condition subject to the shock starting at (ξ_B,ψ_L) gives

$$\psi_{top}=\psi_A-S_r(\xi-\xi_A)+2\sqrt{\psi_L-\psi_A}\sqrt{S_r(\xi-\xi_A)}. \tag{91}$$

The upper shock BC starts at (ξ_B,ψ_L) and propagates downwards, reaching the no-mean-flow line at (ξ_C,ψ_C). Below $\psi=\psi_{u_F}$ the continuation of the shock is unstable by the Lax entropy condition [52] and it breaks into a fan centred at $(\hat{\xi}_C,\hat{\psi}_C)$ in which the concentration

$$\phi_{bottom}=\frac{1}{2}\left(1-\frac{\psi-\psi_C}{S_r(\xi_C-\xi)}\right). \tag{92}$$

The lead $\phi=0$ characteristic CD intersects the $\psi=\psi_L$ particle path again at point D, which has coordinates $\xi_D=\xi_C-(\psi_L-\psi_C)/S_r$. For steady states the breaking segregation wave recirculates large particles on the ψ_L particle

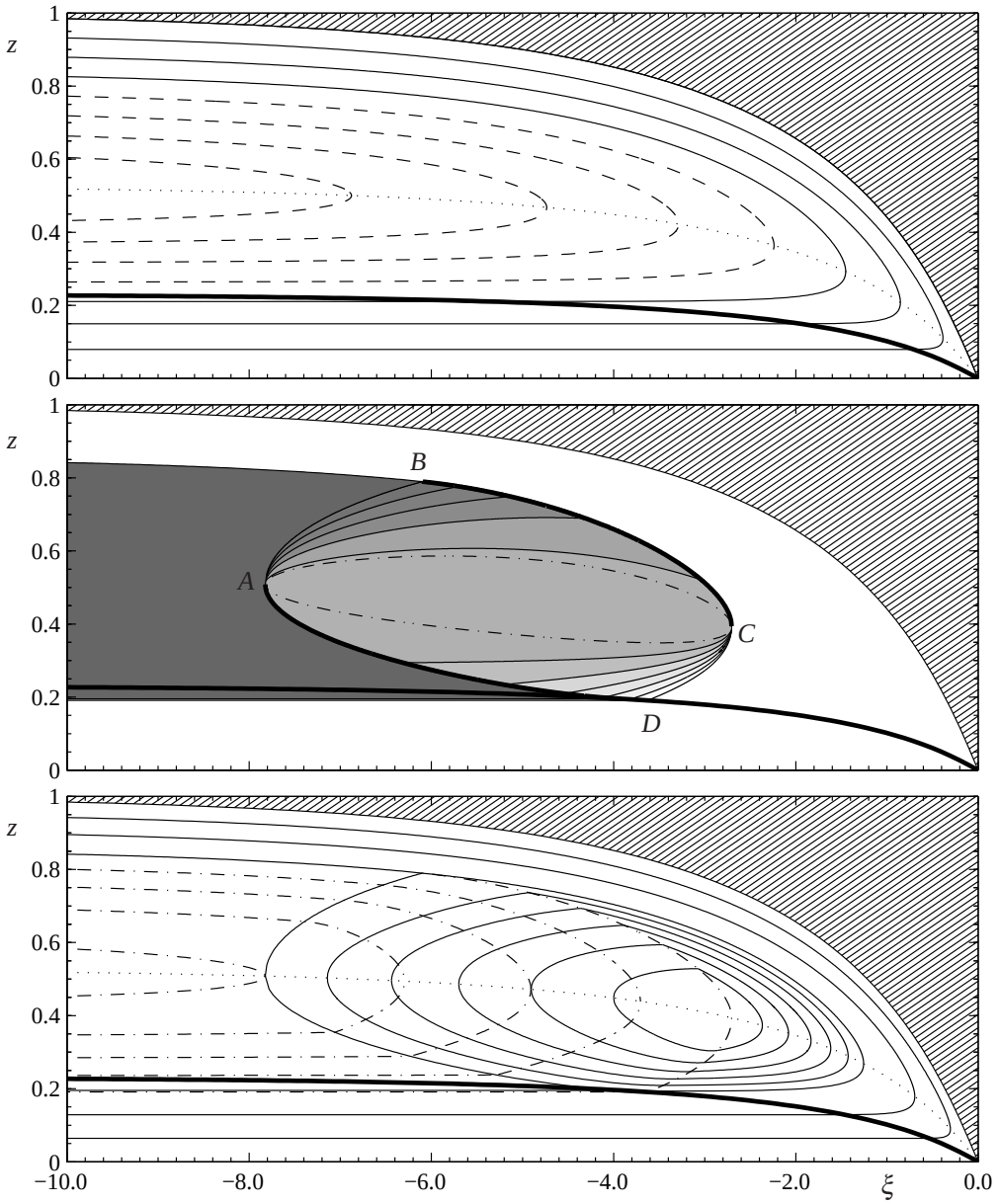

FIGURE 7. The travelling wave solution for the bulk particle paths (top), concentration (middle) and the large and small particle paths (bottom) are shown for an avalanche flow front that is propagating downslope and depositing grains. The deposition surface b is marked by a thick solid line and the dotted line is the no mean flow line z_{u_F}. Thin solid lines are used to indicate bulk flow paths that are deposited, while dashed lines show those paths that recirculate within the avalanche for $\lambda = 0.3$. In the middle panel a breaking size segregation wave ABCD connects an upstream regime that resembles a small particle sandwich, as in figure 6, with a downstream region of purely large grains. There is a "eye" of constant concentration in the centre of the lens, which is marked by a dot-dash line. The concentration is shown using a grey scale with 0.1 unit intervals. Regions of all large particles are white. In the bottom panel the large particle paths are shown with solid lines and small particle paths with dot-dash lines. The inversely graded interface lies along the streamline $\psi_L = -0.1931$ and $S_r = 1$.

path. Part of the path DA also forms a shock across which the small particles separate out, but since the equations for this shock and particle path are identical (89), it is not necessary to determine the location of the transition until later. The large particle path equation adjacent to the fan (92) can be solved subject to the condition that it starts at (ξ_D, ψ_L)

to show that

$$\psi_{bottom} = \psi_C - S_r(\xi_C - \xi) + 2\sqrt{\psi_L - \psi_C}\sqrt{S_r(\xi_C - \xi)}. \tag{93}$$

This intersects with the no-mean-flow line $\psi = \psi_{u_F}$ again at (ξ_A, ψ_A) and breaks into an expansion [52] consistent with our original assumption in equation (90). The small particle sandwich is therefore connected to the large particle front by a breaking size segregation wave as in the middle panel of figure 7. There is an interesting new feature in this case. Since $\psi_A \neq \psi_C$, there is an additional central "eye" of constant concentration

$$\phi_{eye} = \frac{1}{2}\left(1 + \frac{\psi_C - \psi_A}{S_r(\xi_C - \xi_A)}\right), \tag{94}$$

that is bounded above and below by the dot-dash line in the central panel of figure 7. More importantly there is a unique position for the breaking size segregation wave, which connects the upper and lower branches of the ψ_L bulk particle path. If it is too far upstream, part of the lens intersects the basal topography, which violates the assumption that $S_r \neq 0$. While if the lens is too far downstream, not all the large particles above the incoming ψ_L particle path are deposited. The breaking wave must therefore be positioned so that large particles on ψ_L^- are recirculated at the front, while large particles on ψ_L^+ side are deposited. This amounts to the requirement that the ψ_L recirculating particle path is tangent to the basal topography. Gray and Ancey [5] calculated the steady particle paths explicitly, and they are shown in the bottom panel of figure 7. This shows that at steady state all the incoming large particles are deposited, but some of those that had previously reached the front are recirculated, which has been observed in experiment [11, 12]. Most of the small particles are recirculated within the flow, but there are a few that are deposited. Rather intriguingly even though the parent flow is inversely graded, the deposit that is generated by this combination of flow and deposition is normally graded with small particles on top or large. This is diametrically opposite to the inversely graded distribution that is obtained when the flow is brought to rest by a shock wave [15] and raises many questions on the interpretation of deposits that are often made by geologists.

DISCUSSION AND CONCLUSIONS

The segregation-remixing equation (19) provides a simple, but effective way of modelling particle size segregation in granular avalanches. At present little is known about the dependence of the parameters S_r and D_r on the particle size ratio, shear-rate, slope angle and lithostatic pressure, but, both particle dynamics simulations [44] and careful experiments [5], provide important means of calibrating the theory. It may also be possible to find a link with binary kinetic theories [49, 50] as they push towards the dense flow regime. All the results that have been presented in this paper are for a prescribed flow field, but, the theory is sufficiently simple to envisage coupled simulations in which the evolving particle size distribution has a direct feedback on to the bulk flow field, which can be computed with existing avalanche models [7, 25–37]. Such *segregation-mobility* feedback effects are responsible for fingering instabilities in bi-disperse mixtures of dry grains with different frictional properties [11–13], as well as petal formation in rotating drums [18], and the spontaneous formation of leveed channels in both wet and dry geophysical mass flows [6–9, 14].

ACKNOWLEDGMENTS

This research was generously supported by an EPSRC Advanced Research Fellowship GR/S50052/01 & GR/S50069/01 as well as NERC grant NE/E003206/1 and a Royal Society International Travel Grant TG090172.

REFERENCES

1. S. Savage, and C. Lun, *J. Fluid Mech.* **189**, 311–335 (1988).
2. G. Middleton, and M. Hampton, "Subaqueous sediment transport and deposition by sediment gravity flows," in *Marine sediment transport and environmental management*, edited by D. Stanley, and D. Swift, Wiley, 1976, pp. 197–218.
3. R. Bagnold, *Proc. Roy. Soc. Lond. A* **225**, 49–63 (1954).
4. M. Branney, and B. Kokelaar, *Bull Volcanol.* **54**, 504–520 (1992).
5. J. Gray, and C. Ancey, *J. Fluid Mech.* **629**, 387–423 (2009).
6. T. Pierson, "Flow behavior of channelized debris flows, Mount St. Helens, Washington," in *Hillslope Processes*, edited by A. Abrahams, Allen and Unwin, Winchester, Mass., 1986, pp. 269–296.

7. R. Iverson, *Reviews in Geophysics* **35**, 245–296 (1997).
8. V. Jomelli, and P. Bertran, *Geografiska Annaler. Series A, Physical Geography* **83**, 15–28 (2001).
9. P. Bartelt, and B. McArdell, *J. Glaciol.* **55**, 829–833 (2009).
10. R. Iverson, "The debris-flow rheology myth," in *Debris-flow hazards mitigation: Mechanics, prediction and assessment*, edited by D. Rickenmann, and C. Chen, Millpress, Rotterdam, 2003, pp. 303–314.
11. O. Pouliquen, J. Delour, and S. Savage, *Nature* **386**, 816–817 (1997).
12. O. Pouliquen, and J. Vallance, *Chaos* **9**, 621–630 (1999).
13. G. Félix, and N. Thomas, *Earth and Planetary Science Letters* **221**, 197–213 (2004).
14. R. Iverson, and J. Vallance, *Geology* **29**, 115–118 (2001).
15. J. Gray, and K. Hutter, *Continuum Mech. & Thermodyn.* **9**, 341–345 (1997).
16. J. Gray, and V. Chugunov, *J. Fluid Mech.* **569**, 365–398 (2006).
17. K. Hill, G. Gioia, and D. Amaravadi, *Phys. Rev. Lett.* **93**, 224301 (2004).
18. I. Zuriguel, J. Gray, J. Peixinho, and T. Mullin, *Phys. Rev. E* **73**, 061302 (2006).
19. S. Williams, *Powder Technol.* **2**, 13–20 (1968).
20. H. Makse, S. Havlin, P. King, and H. Stanley, *Nature* **386**, 379–382 (1997).
21. J. Gray, and A. Thornton, *Proc. Roy. Soc. A* **461**, 1447–1473 (2005).
22. A. Thornton, J. Gray, and A. Hogg, *J. Fluid Mech.* **550**, 1–25 (2006).
23. C. Truesdell, *Rational Thermodynamics*, Springer, 1984.
24. L. Morland, *Surveys in Geophysics* **13**, 209–268 (1992).
25. S. Grigorian, M. Eglit, and I. Iakimov, *Snow, Avalanches & Glaciers. Tr. Vysokogornogo Geofizich Inst* **12**, 104–113 (1967).
26. S. Savage, and K. Hutter, *J. Fluid Mech.* **199**, 177–215 (1989).
27. J. Gray, M. Wieland, and K. Hutter, *Proc. Roy. Soc. A* **455**, 1841–1874. (1999).
28. M. Wieland, J. Gray, and K. Hutter, *J. Fluid Mech.* **392**, 73–100 (1999).
29. O. Pouliquen, *Phys. Fluids* **11**, 542–548 (1999).
30. R. Iverson, and R. Denlinger, *J. Geophy. Res.* **106**, 553–566 (2001).
31. Y.-C. Tai, S. Noelle, J. Gray, and K. Hutter, *J. Comput. Phys.* **175**, 269–301 (2002).
32. J. Gray, Y. Tai, and S. Noelle, *J. Fluid Mech.* **491**, 161–181 (2003).
33. E. Pitman, C. Nichita, A. Patra, A. Bauer, M. Sheridan, and M. Bursik, *Phys. Fluids* **15**, 3638–3646 (2003).
34. U. Gruber, and P. Bartelt, *Envirn. Model. & Softw.* **22**, 1472–1481 (2007).
35. J. Gray, and X. Cui, *J. Fluid Mech.* **579**, 113–136. (2007).
36. A. Mangeney, F. Bouchut, N. Thomas, J. Vilotte, and M. Bristeau, *J. Geophys. Res.* **112**, F02017 (2007).
37. X. Cui, J. Gray, and T. Johannesson, *J. Geophys. Res.* **112**, F04012 (2007).
38. G. Kynch, *Trans. Faraday Soc.* **48**, 166–176 (1952).
39. H.-K. Rhee, R. Aris, and N. Amundson, *First-order partial differential equations: Volume 1 Theory and applications of single equations*, Prentice-Hall, Englewood Cliffs, New Jersey, 1986.
40. J. Vallance, and S. Savage, "Particle segregation in granular flows down chutes„" in *IUTAM Symposium on segregation in granular materials*, edited by A. Rosato, and D. Blackmore, Kluwer, 2000.
41. G. Whitham, *Linear and nonlinear waves.*, John Wiley, New York, 1974.
42. V. Dolgunin, and A. Ukolov, *Powder Technol.* **83**, 95–103 (1995).
43. D. Khakhar, J. McCarthy, and J. Ottino, *Phys. Fluids* **9**, 3600–3614 (1997).
44. D. Khakhar, J. McCarthy, and J. Ottino, *Chaos* **9**, 594–610 (1999).
45. P. Rognon, J. Roux, M. Naaim, and F. Chevoir, *Phys. Fluids* **19**, 058101 (2007).
46. E. Linares-Guerrero, C. Goujon, and R. Zenit, *J. Fluid Mech.* **593**, 475–504 (2007).
47. S. Hajra, and D. Khakhar, *Phys. Rev. E* **69**, 031304 (2004).
48. J. Jenkins, and F. Mancini, *J. Appl. Mech.* **54**, 27–34 (1987).
49. J. Jenkins, "Particle segregation in collisional flows of inelastic spheres," in *Physics of dry granular media*, edited by H. Herrmann, J.-P. Hovi, and S. Luding, NATO ASI series, Kluwer, 1998.
50. J. Jenkins, and D. . Yoon, *Phys. Rev. Lett.* **88**, 194301–4 (2001).
51. P. Chadwick, *Continuum Mechanics. Concise theory and problems*, George Allen & Unwin, 1976.
52. M. Shearer, J. Gray, and A. Thornton, *European J. Applied Math.* **19**, 61–86 (2008).
53. J. Cole, *Q. Appl. Maths* **9**, 225–236 (1951).
54. E. Hopf, *Comm. Pure Appl. Math.* **3**, 201–230 (1950).
55. J. Gray, M. Shearer, and A. Thornton, *Proc. Roy. Soc. A* **462**, 947–972 (2006).
56. A. Thornton, and J. Gray, *J. Fluid Mech* **596**, 261–284 (2008).
57. M. McIntyre, E. Rowe, M. Shearer, J. Gray, and A. Thornton, *A.M.R.X.* **2007**, abm008 (2007).
58. H. Herrmann, "On the shape of a sandpile," in *Physics of dry granular media*, edited by H. Herrmann, J. Hovi, and S. Luding, NATO ASI series, Kluwer Academic, 1998, pp. 697–702.
59. J. Baxter, U. Tüzün, D. Heyes, I. Hayati, and P. Fredlund, *Nature* **391**, 136 (1998).
60. J. Gray, *J. Fluid Mech.* **441**, 1–29 (2001).
61. O. Pouliquen, and Y. Forterre, *J. Fluid Mech.* **453**, 133–151 (2002).
62. M. Abramowitz, and I. Stegun, *Handbook of Mathematical Functions*, Dover, 1970, p. 3.3.7, 9 edn.